Snake orbits and related magnetic edge states

2000 J. Phys.: Condens. Matter 12 9771

(http://iopscience.iop.org/0953-8984/12/47/305)

J. Phys.: Condens. Matter **12** (2000) 9771–9786. Printed in the UK PII: S0953-8984(00)14768-X

Snake orbits and related magnetic edge states

J Reijniers and F M Peeters

Departement Natuurkunde, Universiteit Antwerpen (UIA), Universiteitsplein 1, B-2610 Antwerpen, Belgium

E-mail: peeters@uia.ua.ac.be

Received 15 June 2000, in final form 10 October 2000

Abstract. We study the electron motion near magnetic field steps at which the strength and/or sign of the magnetic field changes. The energy spectrum for such systems is found and the electron states (bound and scattered) are compared with their corresponding classical paths. Several classical properties such as the velocity parallel to the edge, the oscillation frequency perpendicular to the edge and the extent of the states are compared with their quantum mechanical counterparts. A class of magnetic edge states is found which do not have classical counterparts.

1. Introduction

The transport properties of a two-dimensional electron gas (2DEG) subjected to a non-homogeneous perpendicular magnetic field (periodically modulated or not) have been the focus of a great deal of research in recent years [1]. Current fabrication technologies permit one to create non-homogeneous magnetic fields on a nanometre scale by deliberately shaping or curving the 2DEG [2], or by integration of superconducting [3, 4] or ferromagnetic materials [5, 6] on top of the 2DEG. This will add a new functional dimension to the present semiconductor technology and will open avenues for new physics and possible applications [7].

Theoretically, the effects of non-homogeneous magnetic fields on a 2DEG have been studied both in the ballistic and in the diffusive regime. The resulting perpendicular magnetic field can act as a scattering centre [5, 6, 8], but can also bind electrons [9–12], and so influence the transport properties of the 2DEG. In transport calculations one needs the electron states, which are obtained by solving the Schrödinger equation.

Müller [13] studied theoretically the single-particle electron states of a 2DEG in a wide quantum waveguide under the application of a non-uniform magnetic field and showed that in the case of a magnetic field modulation in one direction, transport properties also become one dimensional and electron states propagate perpendicularly to the field gradient.

Making use of this decoupling, the electron states for different non-homogeneous magnetic field profiles along one dimension were investigated, i.e. for a periodically modulated magnetic field [14–16], for magnetic quantum steps, barriers and wells in an infinite 2DEG [17, 18] and in a narrow waveguide [19].

In this paper we consider an infinite 2DEG subjected to a step-like magnetic field, i.e. abruptly changing in magnitude or polarity at $x = 0$, in one dimension (taken to be the x-direction). Preliminary results were presented in reference [20]. First the situation for two opposite homogeneous magnetic fields with the same strength will be considered. The classical trajectories correspond to *snake orbits* and were already used in the 1970s [21] to describe

0953-8984/00/479771+16$30.00

electron propagation parallel to the boundary between two magnetic domains. Back then, one was interested in understanding the electron transport through multi-domain ferromagnets and it turned out to be more convenient to work with the classical trajectories than with the corresponding electron states, which allows one to use a semi-classical theory which reduces the complexity of the theory considerably. We are interested in transport through a 2DEG situated in a semiconductor in which the Fermi energy is orders of magnitude smaller than in the metallic systems of reference [21].

We will study thoroughly the quantum mechanics of such electron states in a 2DEG subjected to this step magnetic field profile, and we will compare them with their classical counterparts. We will discuss the energy spectrum and the corresponding electron states, and derive several properties. We will show the existence of states which have a velocity in the opposite direction to what one would expect classically. Additionally, we will show that adding a background magnetic field modifies the spectrum and the states considerably.

The paper is organized as follows. In section 2 we present our theoretical approach. In section 3 we calculate the energy spectrum, the wavefunctions and their corresponding group velocity, and compare them with their quantum mechanical counterparts. In section 4 we study the influence of a background magnetic field on the quantum mechanical and classical behaviour. In section 5 we focus on the negative-velocity state and finally, in section 6, we construct time-dependent states, and interpret them classically for several magnetic field profiles.

2. Theoretical approach

We consider a system of non-interacting electrons moving in the xy-plane in the absence of any electric potentials. The electrons are subjected to a magnetic field profile $\vec{B} = (0, 0, B_z(x))$. First, we will study the electronic states near the edge of two magnetic fields with the same strength but opposite sign:

$$B_z(x) = B_0[2\theta(x) - 1] \tag{1}$$

which is independent of the y-coordinate. Next, we will consider the influence of a background magnetic field B on these states, which results in the magnetic field profile

$$B_z(x) = B_0[2\theta(x) - 1] + B. \tag{2}$$

In the following we will use $B^l = B_z(x < 0)$ and $B^r = B_z(x > 0)$ to denote respectively the magnetic field on the left-hand side and the right-hand side of the magnetic edge.

The one-particle states in such a 2DEG are described by the Hamiltonian

$$H = \frac{1}{2m_e} p_x^2 + \frac{1}{2m_e}\left[p_y - \frac{e}{c}A(x)\right]^2. \tag{3}$$

Taking the vector potential in the Landau gauge,

$$\vec{A} = (0, xB_z(x), 0) \tag{4}$$

we arrive at the following 2D Schrödinger equation:

$$\left\{\frac{\partial^2}{\partial x^2} + \left[\frac{\partial}{\partial y} + \mathrm{i}xB_z(x)\right]^2 + 2E\right\}\psi(x, y) = 0$$

where the magnetic field is expressed in units of B_0, all lengths are measured in units of the magnetic length $l_B = \sqrt{\hbar c/eB_0}$, energy is measured in units of $\hbar\omega_c$, with $\omega_c = eB_0/m_e c$ the

cyclotron frequency, and the velocity is expressed in units of $l_B\omega_c$. H and p_y commute due to the special form of the gauge, and consequently we can write the wavefunction as follows:

$$\psi(x, y) = \frac{1}{\sqrt{2\pi}} e^{-iky} \phi_{n,k}(x) \tag{5}$$

which reduces the problem to the solution of the 1D Schrödinger equation

$$\left[-\frac{1}{2} \frac{d^2}{dx^2} + V_k(x) \right] \phi_{n,k}(x) = E_{n,k} \phi_{n,k}(x) \tag{6}$$

where it is the k-dependent effective potential

$$V_k(x) = \frac{1}{2} \left[x B_z(x) - k \right]^2 \tag{7}$$

which contains the two dimensionality of the problem. We will solve equation (6) numerically by use of a discretization procedure. In some limiting cases, analytical results can be obtained.

3. In the absence of a background magnetic field

Let us first consider the case where no background magnetic field is present. The situation is then symmetric, and easier to solve. The effective potential for this case is shown in figure 1(a) for $k = -2$ (dotted curve) and $k = 2$ (solid curve). We notice from equation (7) that this potential is built from two parabolas, with minima situated at $x^l = -k$, and $x^r = k$, thus respectively on the left-hand side and right-hand side of the magnetic edge. The total potential has for $k > 0$ two local minima respectively at $x = -k$ and $x = +k$, while for $k < 0$ it has only one minimum at $x = 0$. Before we describe the energy spectrum of the snake orbits and their corresponding properties, we first discuss the limiting behaviour.

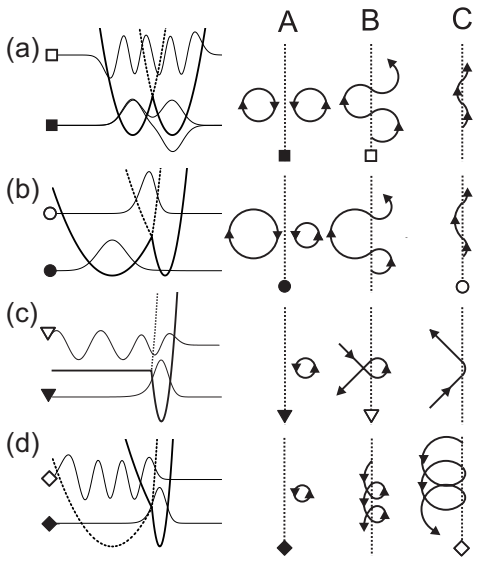

Figure 1. The effective potential (left-hand part of the figure) for $k = -2$ (dotted curve) and $k = 2$ (solid curve) for the different magnetic field profiles (B^l, B^r): (a) $(-1, 1)$, (b) $(-0.5, 1.5)$, (c) $(0, 2)$, (d) $(0.5, 2.5)$, indicated at the top of figure 2. The wavefunctions corresponding to the states in figure 2, as indicated by the corresponding symbols, are also shown. Also given is the schematic representation of the classical electron trajectories (right-hand part of the figure) corresponding to the different regions indicated in figure 2.

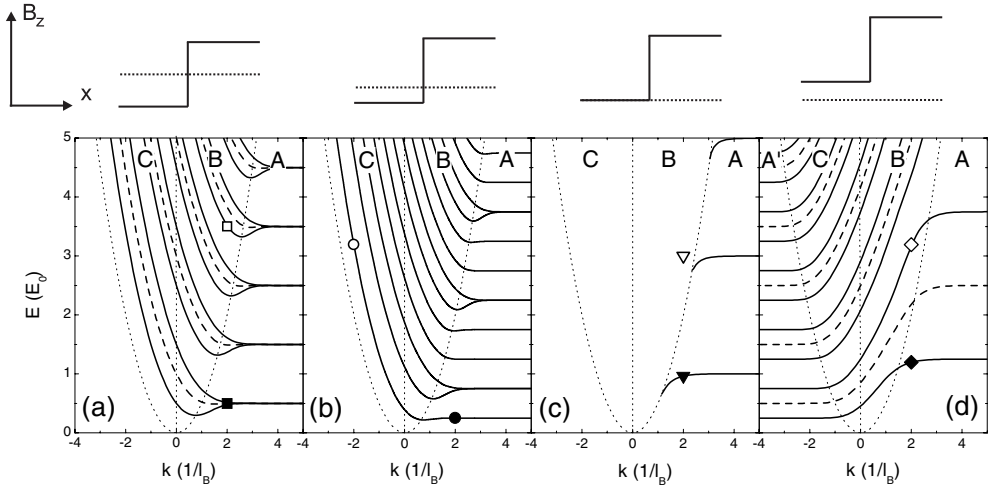

Figure 2. The energy spectra for different magnetic field profiles (B^l, B^r) shown at the top of the figure: (a) (−1, 1), (b) (−0.5, 1.5), (c) (0, 2), (d) (0.5, 2.5). The dotted curves mark the different classical regions. The dashed curves in (a) and (b) show the average energy of two adjacent levels. The symbols correspond to the electron wavefunctions plotted in figure 1.

3.1. Limiting behaviour for $k \to \pm\infty$

For $k \to \infty$, the minima of the parabolas are situated far from each other. The electrons are in the Landau states of two opposite magnetic fields, one on the left, the other on the right, and they are not interacting with each other. The electron wavefunctions are given by

$$\langle L|x\rangle = C_m H_m(x+k)\mathrm{e}^{-(x+k)^2/2} \qquad \langle R|x\rangle = C_m H_m(x-k)\mathrm{e}^{-(x-k)^2/2}$$

respectively, where $H_m(x)$ is the Hermite polynomial. For decreasing k the parabolas shift towards each other, and the electrons will start to 'feel' each other. In terms of wavefunctions, this results in a parabolic cylinder function $\phi(x) = D_{E-1/2}[\sqrt{2}(x-k)]$ matched at $x = 0$, with the condition that

$$\frac{\mathrm{d}}{\mathrm{d}\alpha} D_{E-1/2}(\alpha)\big|_{\alpha=-\sqrt{2}k} = 0 \qquad \text{or} \qquad D_{E-1/2}(-\sqrt{2}k) = 0$$

for the symmetric and the antisymmetric wavefunction, respectively. This leads to a change in energy of the electron states, which can be understood as a lifting of the degeneracy of the two original electron wavefunctions. The energy can then be written as

$$E_\pm(k) = \langle L|H|L\rangle(k) \pm \langle L|H|R\rangle(k) = E(k) \pm \Delta E(k)$$

with the corresponding wavefunctions $|\phi\rangle = |R\rangle \mp |L\rangle$. One can see that for an electron confined in one parabola, the presence of the other parabola results in two effects: (1) a decrease of $E(k)$ due to the finite presence of the wavefunction in the other parabola; and (2) a splitting of the energy level due to the overlap, i.e. one level (E_+) shifts upwards, while the other (E_-) shifts down. For $k \to \infty$, this results in the following first-order approximations to E and ΔE:

$$E_m(k) = \frac{1}{2} + m - \frac{2^{m-1}}{m!\sqrt{\pi}} k^{2m-1}\mathrm{e}^{-k^2} \tag{8a}$$

$$\Delta E_m(k) = \frac{2^m}{m!\sqrt{\pi}} \mathrm{e}^{-k^2} k^{2m+1}. \tag{8b}$$

In the other limit $k \to -\infty$, the effective potential can be approximated by a triangular well $V(x) = k^2/2 - kB_0x$. Solutions for this potential consist of Airy functions, again matched at $x = 0$, with the condition that $\phi'(0) = 0$ or $\phi(0) = 0$ which results respectively in the antisymmetric wavefunction

$$\phi_{2m}(x) = C_{2m}(k)(|x|/x)\,\mathrm{Ai}[z_{\mathrm{Ai}',m+1} + (2k)^{1/3}|x|]$$

and a symmetric one

$$\phi_{2m+1}(x) = C_{2m+1}(k)\,\mathrm{Ai}[z_{\mathrm{Ai},m+1} + (2k)^{1/3}|x|]$$

respectively with energy

$$E_{2m}(k \to -\infty) = \frac{1}{2}\left[k^2 - z_{\mathrm{Ai}',m+1}(2|k|)^{2/3}\right] \tag{9a}$$

$$E_{2m+1}(k \to -\infty) = \frac{1}{2}\left[k^2 - z_{\mathrm{Ai},m+1}(2|k|)^{2/3}\right] \tag{9b}$$

where $z_{\mathrm{Ai},n}$ $(=-2.338, -4.088, -5.521, \ldots, -[3\pi(4n-1)/8]^{2/3})$ and $z_{\mathrm{Ai}',n}$ $(=-1.019, -3.248, -4, 820, \ldots, -[3\pi(4n-3)/8]^{2/3})$ denote respectively the nth $(n = 1, 2, 3, \ldots, \infty)$ zero of the Airy function and that of its derivative. One can see that for increasing negative k, the difference between the two energy branches increases, and is to first order linear in $|k|$. That is, the more negative k, the narrower the well, and thus the more the energy levels are shifted away from each other.

3.2. Spectrum and velocity

Solving equation (6) numerically gives rise to the energy spectrum shown (solid curves) in figure 2(a). For $k = \infty$, we obtain the earlier-mentioned Landau levels, which are labelled with the quantum number m. Each level is twofold degenerate. For decreasing k, the degeneracy is lifted and they separate into two different branches with eigenstates $|2m\rangle$ and $|2m+1\rangle$ and eigenvalues E_{2m} and E_{2m+1}, and corresponding quantum numbers $n = 2m$ and $n = 2m+1$. This quantum number n not only results from arranging the levels according to their lowest energy, starting with $n = 0$, but also reflects the number of nodes of the corresponding wavefunction. Notice that the levels have now a non-zero derivative, i.e. electrons propagate in the y-direction, and their group velocity is given by $v(k) = -\partial E(k)/\partial k$. (The minus sign appears here because in equation (5) we took $k_y = -k$.) This group velocity is plotted (solid curves) in figure 3(a) for the six lowest levels. For $k = \infty$, electrons are in a Landau level, and consequently there is no net current in the y-direction. Decreasing k results in a net current in the y-direction, which is positive for the upper branches $(2m+1)$, but is initially negative for the branches $(2m)$. For more negative values of k it increases almost linearly with increasing $|k|$; this becomes the first-order analytical result $v_m(k \to \infty) = -k$, obtained by differentiating (9*a*) and (9*b*).

3.3. Classical picture

The centre of the classical orbit corresponds to a zero in the effective potential. The energy spectrum can be divided up into three regions which can be classically understood by considering the electron orbits drawn in figure 1(a). In region A the electrons move in closed orbits either in the magnetic field on the left-hand side or in that on the right-hand side. Since its cyclotron radius is smaller than the distance to the magnetic field discontinuity, they 'feel' a homogeneous magnetic field. As a result of the opposite magnetic field, one electron rotates clockwise, while the other moves anticlockwise. There is no net velocity. In region B

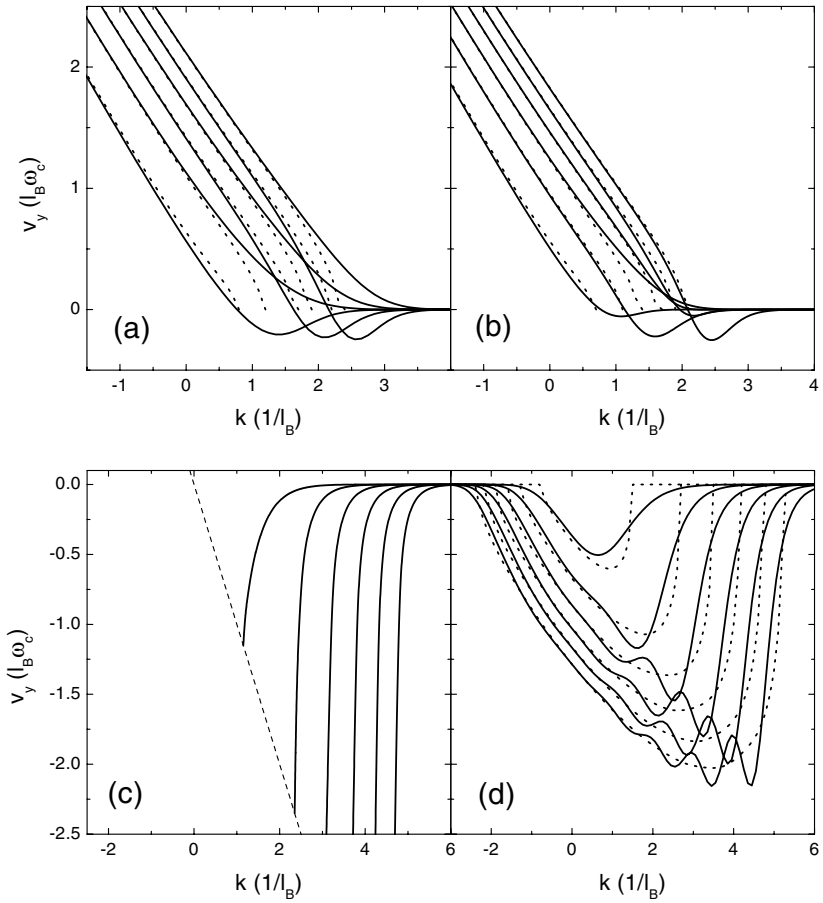

Figure 3. The group velocity in the y-direction (parallel to the edge) of the six lowest branches of figure 2 for the different magnetic field profiles ((a), (b), (c), (d)). The dotted curves correspond to the velocities calculated for the classical snake orbits.

the cyclotron radius intersects the magnetic field discontinuity slightly, i.e. in such a way that the moving electron and the centre of its orbit are on the same side. The electron is able to penetrate into the opposite magnetic field region, which results in a (rather small) propagation in the y-direction, $v_y > 0$. For $k = 0$ the centre of the orbit is exactly on the edge between the two opposite magnetic fields. In region C the centre of the cyclotron orbit is located in the magnetic field region opposite to that in which the electron is moving, resulting in a faster propagation of the electron in the y-direction. These different regions are also indicated in figure 2(a).

We can also make a quantitative classical study of the velocity, starting from the quantum mechanical energy spectrum. Since in classical mechanics there is no quantization, we make use of the quantum energy spectrum obtained in order to find the classical energy and thus the radius of the cyclotron orbit. Classically, the energy is contained in the circular velocity v_φ through $E(k) = v_\varphi^2(k)/2$. For any given quantum mechanical value of $E(k)$ we obtain classically the circular velocity $v_\varphi(k) = \sqrt{(2E(k))}$. Now if we consider $x_0 = \pm k$ to be the centre of the electron orbit, we can calculate for every k-value the classical velocity $v_y(k)$, since we also know $v_\varphi(k)$ and the cyclotron radius $R(k) = v_\varphi(k)$. Using geometrical considerations,

we obtain the following relation:

$$v_y(k) = v_\varphi(k)\sqrt{1-[k/v_\varphi(k)]^2}\Big/ \arccos[k/v_\varphi(k)] \tag{10}$$

which is shown in figure 3(a) by the dotted curves. Comparing this with its quantum mechanical counterpart, we notice that for $k < 0$ good agreement is found, but for $k > 0$ there is a large discrepancy. Moreover, one can see that negative velocities cannot exist classically.

The critical k-value, k^*, defines the region for which no classical propagating state can exist, i.e. when the electron describes just a circular orbit in a homogeneous magnetic field and does not intersect the magnetic field discontinuity. Hence, this critical value has to be equal to the cyclotron radius

$$k^* = R(k^*) = v_\varphi(k^*) = \pm\sqrt{2E(k^*)}$$

which leads to the boundary drawn in figure 2(a) (dotted parabola).

4. With a background magnetic field

With a background magnetic field three different configurations: (a) $0 < B < B_0$; (b) $B = B_0$; and (c) $B_0 < B$ have to be considered. In the following we will study the snake orbits in these configurations.

4.1. $0 < B < B_0$

Applying a background magnetic field $0 < B < B_0$ results in a situation which is very similar to the previous one. Again the two magnetic fields have opposite sign, but in this case they also have different strength, i.e. $B^l = -B^r/p$. Again we can calculate analytically the correction to the energy in the limit $k \to \infty$. For an electron on the right-hand side in the mth Landau state of a magnetic field with strength $B^r = B_0$, the deviation from the Landau energy due to the presence of the other parabola in the effective potential is given by a matrix element, which to second-order reads

$$E_m(k \to \infty) = |\langle R|H|R\rangle(k)| = \left[m + \frac{1}{2}\right] - \frac{2^{m-2}}{m!\sqrt{\pi}}\left(1 + \frac{1}{p}\right)k^{2m-1}\mathrm{e}^{-k^2}. \tag{11}$$

For an electron on the left-hand side, i.e. in the smaller-magnetic-field $B^l = -B_0/p$ region, in the mth Landau level, this results in

$$E_m(k \to \infty) = |\langle L|H|L\rangle(k)| = \frac{1}{p}\left[m + \frac{1}{2}\right] - \frac{2^{m-2}}{m!\sqrt{\pi}}\left(1 + \frac{1}{p}\right)k^{2m-1}\mathrm{e}^{-k^2}. \tag{12}$$

Also in this case the energy is smaller than the corresponding Landau energy. The downward energy shift decreases for increasing p.

If p is an integer, Landau states on the left-hand side and the right-hand side, respectively with quantum number pm and m, coincide for $k \to \infty$. As a consequence these states have an overlap, which reads to first order

$$\langle L|H|R\rangle = (-1)^{m+1}2^{m(p+1)/2}\left(\frac{1}{(pm)!m!\pi}\right)^{1/2} p^{pm/2}\mathrm{e}^{-k^2(1+p)/2}k^{m(p+1)+1}. \tag{13}$$

One can see that for decreasing magnetic field, i.e. increasing p, this function decreases because of the exponential factor. The electron wavefunction in the lower-magnetic-field region is extended over a larger region, and further away from the other (with the centre at kp). The overlap therefore decreases with increasing p. As a result of this, the energy for $k \to \infty$ and $p > 1$ is given by $\langle R|H|R\rangle$ and $\langle L|H|L\rangle$.

For $p = 1$, we obtain the previous result, but for increasing p, the second-order term in equations (11) and (12) becomes more important than equation (13), because of the exponential factor. The splitting is lifted, and the main contribution to the negative velocity for $k \to \infty$ arises from equation (13) due to the finite extent of the wavefunction in the other parabola.

As an example we studied numerically the case where a background magnetic field $B = B_0/2$ is applied, i.e. $B^l = -B_0/2$ and $B^r = 3B_0/2$. As one can see in figure 1(b), this results in two parabolas with different minima and confinement strengths. The resulting spectrum (see figure 2(b)) is very similar to the one of the previous case, but unlike in the previous symmetrical case, not all states are twofold degenerate for $k \to \infty$. We now obtain two different sets of Landau states, corresponding to electrons moving in different magnetic field regions with different strengths. In this case the second Landau level on the left coincides with the first on the right. The classical picture for the three different regions corresponds to the one drawn in figure 1(b), and is also similar to the previous case, except for the different cyclotron radii. With this picture in mind, one can again calculate the classical velocity, which turns out to be identical to equation (10). From figure 3(b) we notice that again we obtain good agreement for $k > 0$, but for $k < 0$ there is a large discrepancy. The negative velocity can in this case also not be explained classically.

The critical k-value $k^* = \sqrt{(2E(k^*))}$ for which snake orbits are classically possible are indicated by the parabola in figure 2(b).

4.2. $B = B_0$

When a background magnetic field $B = B_0$ is applied, we obtain the magnetic barrier studied in reference [17], where the magnetic field is different from zero only in the region $x > 0$, i.e. $B^l = 0$ and $B^r = 2B_0$. From figure 1(c) one can see that in this case the potential is made up of only one parabola on the right-hand side; on the left-hand side it is constant: $k^2/2$. The energy spectrum and corresponding velocities for this particular case are shown in figures 2(c) and 3(c), respectively. We notice that for $k \to \infty$ we again obtain Landau states, which correspond to bound states on the right-hand side of the magnetic edge. Consistently, as this is a limiting case of the former magnetic field states, i.e. for $p = \infty$, the energy decreases with decreasing k and there is no splitting of the energy levels. Thus now we only have states which propagate with negative velocity to which we cannot assign a classical interpretation.

Also in this case we can subdivide the spectrum into three regions: (A) the electrons move in closed orbits in the magnetic field region on the right-hand side, (B) electrons are free, propagate forward and are reflected on the barrier and (C) electrons are free, propagate backward and are reflected on the magnetic edge. Notice that for a free electron, the energy is larger than $k^2/2$, since now the electron also propagates in the x-direction and consequently has an additional kinetic energy $k_x^2/2$.

Classically, propagating states in the magnetic field region do not exist; there are only Landau states. The boundary where these classical trajectories are possible is again given by $k^* = \sqrt{(2E(k^*))}$.

4.3. $B_0 > B$

By applying a background magnetic field with strength larger than $B > B_0$, we arrive at the situation where $0 < B^l < B^r$. The magnetic fields on the left-hand side and the right-hand side have the same sign, but different strengths, i.e. $B^l = B^r/p$.

To obtain the energy in the limits $k \to \pm\infty$, we can again approximate the wavefunction as being in a Landau state in the corresponding magnetic field. We found

$$E(k \to \infty) = \langle R|H|R\rangle(k) = \left[m + \frac{1}{2}\right] - \frac{2^{m-2}}{m!\sqrt{\pi}}\left(1 + \frac{1}{p}\right)k^{2m-1}\mathrm{e}^{-k^2} \tag{14}$$

for an electron on the right-hand side in the mth Landau state of a magnetic field with strength $B^r = B_0$. For an electron on the left-hand side, in the smaller magnetic field $B^l = B_0/p$ in the mth Landau level, we have

$$E(k \to -\infty) = \langle L|H|L\rangle(k) = \frac{1}{p}\left[m + \frac{1}{2}\right] + \frac{2^{m-2}}{m!\sqrt{\pi}}\left(1 + \frac{1}{p}\right)k^{2m-1}\mathrm{e}^{-k^2} \tag{15}$$

which results in a negative velocity.

The energy spectrum and the velocity of these eigenstates for the case where $B = 3B_0/2$, i.e. $B^l = B_0/2$, $B^r = 5B_0/2$, are plotted respectively in figures 2(d) and 3(d). The centre of the orbit is situated on the right-hand side for $k > 0$; for $k < 0$ it is on the left-hand side. For $k \to \pm\infty$, the electrons move in a homogeneous magnetic field (on the left-hand side ($k \to -\infty$) or right-hand side ($k \to +\infty$) of $x = 0$), and thus $v_y = 0$.

From figure 1(d) one notices that there is only one minimum in the effective potential. This is due to the fact that the two different parabolas (corresponding to the different magnetic fields) which constitute the effective potential have their minima on the same side, i.e. on the left-hand side ($k < 0$) or on the right-hand side ($k > 0$). The trajectories corresponding to regions A, B and C are depicted in figure 1(d). The trajectories in region A′ are similar to those in A but now for a magnetic field on the left-hand side, i.e. with smaller strength.

Geometrical considerations yield the following classical velocity:

$$v_y(k) = 2v_\varphi(k)\sqrt{1 - \left[k/v_\varphi(k)\right]^2}\left\{B^l \arccos\left[-k/v_\varphi(k)\right] + B^r \arccos\left[k/v_\varphi(k)\right]\right\}^{-1} \tag{16}$$

which is plotted in figure 3(d) as dotted curves together with the quantum mechanical group velocity. One can see that, in contrast to the previous cases, the negative velocity can be understood as classical snake orbits, but these snake orbits all run in the same y-direction and now there are no states with $v_y > 0$.

Notice that the quantum mechanical velocity exhibits a small oscillatory behaviour on top of a uniform profile. These wiggles can be understood from the electron distribution over the two parabolas (see figure 4). With increasing k, the electron distribution is shifted from the left-hand parabola to the right-hand one. Due to the wavelike character of this distribution, the probability for an electron to be in the right-hand parabola (the integrated solid region in the inset of figure 4) exhibits wiggles as a function of k, with n maxima as shown in figure 4. Energetically it is favourable for an electron state to have as much electron probability as possible in the lower-potential region. Consequently, when the electron probability in the lower-potential region attains a maximum, a maximum downward energy shift will be introduced on top of the overall energy change, and this will result in a maximum in the group velocity.

5. Negative-velocity states

Formally, the existence of the quantum mechanical negative-velocity state can be attributed to the fact that shifting two one-dimensional potential wells towards each other results in a significant rearrangement of the energy levels in the composite potential well. Because the composed well is broader, some states, e.g. the ground state, have an energy which is lower

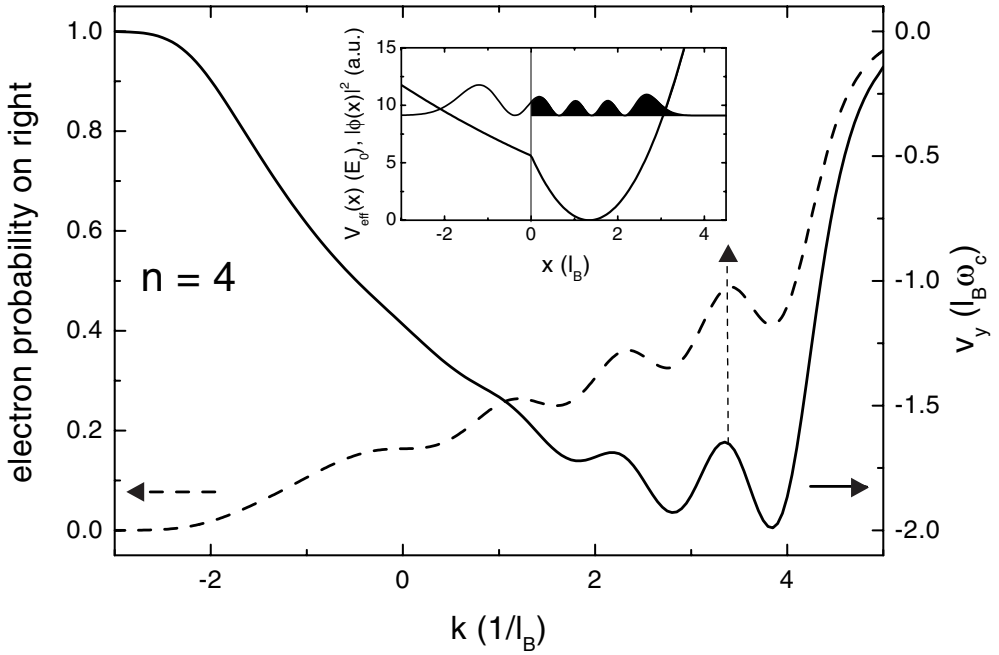

Figure 4. The velocity for the $n = 4$ state of figure 3(d), and the electron probability for the electron to be in the right-hand part of the parabola as a function of k. The inset shows the effective potential and the electron probability at the local maximum $kl_B = 3.4$.

than those in each of the individual narrower wells. In this particular case, the wave vector k measures the distance of the two wells from each other, and consequently this energy decrease results in a negative group velocity $-\partial E/\partial k$. In this section we focus on these negative-group-velocity states.

Since the negative-velocity states are present for any background magnetic field B, but can only be understood classically in the situation where $B > B_0$, we will investigate the group velocity for a fixed k-value with varying background magnetic field. In figure 5 the spectrum is plotted as a function of the applied background field B. We have chosen $k = 1.5$ because in this case a large negative velocity is obtained for the lowest level when $B = 0$. Notice that for $B < B_0$:

(1) Almost all levels decrease in energy with increasing background field.
(2) There is an anti-crossing for $E/E_0 = 0.4 + 0.458B/B_0$ (dotted line). This anti-crossing occurs when $B/B_0 = n/(n+1)$, with n the Landau level index. For this condition some of the Landau levels are degenerate in the limit $k \to \infty$ (see figure 2(b) for the case $n = 0$).
(3) For $B \to B_0$ the separation between the levels decreases to zero and a continuous spectrum is obtained with a separate discrete level at the anti-crossing line.

The continuous spectrum for $B = B_0$ results from the scattered states in the potential of figure 2(c), while the discrete state is the bound state in this potential. For the k-value considered, i.e. $k = 1.5$, only one bound state is found for $B = B_0$.

The corresponding group velocity $v_y = -\partial E/\partial k$ is shown in figure 6. Notice that the maximum negative velocity is obtained near the anti-crossings in the energy spectrum (figure 5). Near $B/B_0 = n/(n+1)$ the splitting in the energy spectrum (see figure 2) is largest and as a

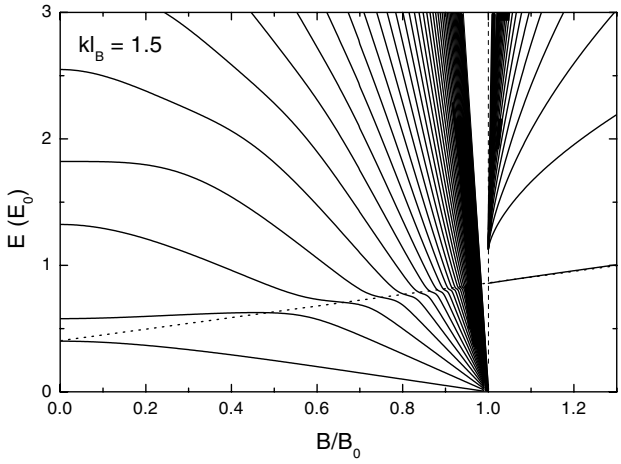

Figure 5. The energy spectrum at $kl_B = 1.5$ for the 40 lowest states as a function of the applied background field B/B_0.

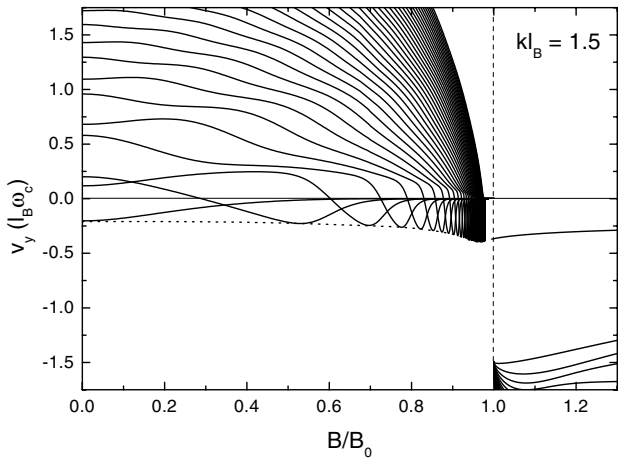

Figure 6. The group velocity v_y as a function of B/B_0, corresponding to the electron states of figure 5.

consequence one of the levels is pushed strongly down in energy and consequently v_y becomes strongly negative. Notice that: (1) every level has some B/B_0 region in which $v_y < 0$ and (2) for $B/B_0 \to 1$ the velocity $v_y \to 0$, while (3) the envelope of $(v_y)_{\min}$ in figure 6 reaches, for B/B_0, the $v_y < 0$ value of the $B = B_0$ state. For $B > B_0$ we have $v_y < 0$ for all states.

Using expressions (10) and (16), we can also calculate the classical velocity corresponding to the energy spectrum in figure 5. This is shown in figure 7. We notice that for $B/B_0 < 1$, the classical velocity has a similar behaviour to the quantum mechanical one, except for the anti-crossings and the lack of negative velocities, which do not have classical counterparts. These negative velocities appear suddenly for $B/B_0 > 1$ and exhibit more or less the same behaviour.

As was already apparent from the above study, a necessary condition for the existence of the non-classical edge states is the presence of two local minima in the effective potential. In

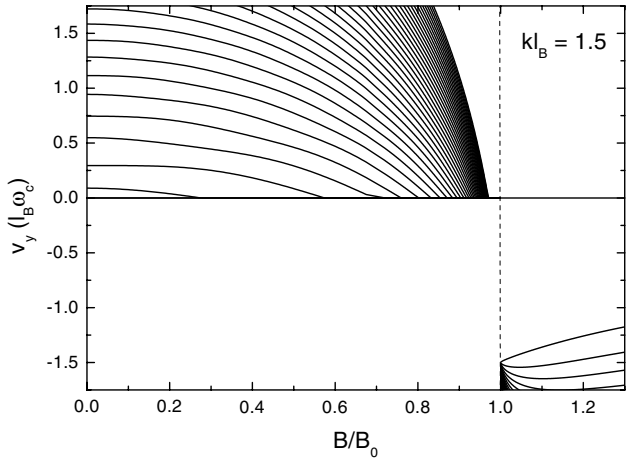

Figure 7. The classical velocity in the y-direction as a function of B/B_0, corresponding to the electron states of figure 5.

the limiting case $B = B_0$ the second minimum is the limiting case of a flat region in $V_k(x)$ for $x < 0$. But not all of these states have a negative velocity. How can we classify them?

From figures 2(a), 2(b) one notices that initially (for rather small B-values) the parabola $E = k^2/2$ separates the region where only states with positive group velocity exist from the region where negative-velocity states are also present. This is due to the fact that the value of this parabola equals the height of the barrier between the two parabolic wells for the corresponding k-value. When the energy exceeds this barrier, the shape of the wavefunction is not determined any longer by the separate parabolas, but is now determined by the overall composite well width. For decreasing k the well is squeezed, and thus all of the energy levels are pushed upwards, resulting in a positive group velocity. Although this is not an exact rule and cannot be extended rigorously throughout the $B < B_0$ regime, it nevertheless provides insight into the k-values (or B-values) for which these negative-velocity states arise.

Inspection of the wavefunctions shows that there is a feature which marks the negative-velocity states, and which relates indirectly to the presence of the different potential wells. It turns out that if the wavefunction or its first derivative exhibits a dip at some x which satisfies $\phi(x)\phi''(x) > 0$ and $\phi'(x) = 0$, or $\phi'(x)\phi'''(x) > 0$ and $\phi''(x) = 0$ and the condition that $\phi(x) \neq 0$, then the state has a non-classical negative velocity. This is true for every k-value, as long as $B < B_0$. This is illustrated in figure 8 where we plot the wavefunction for $k = 1.5$, $n = 2$, with background magnetic field $B/B_0 = 0.68$ and 0.73. The above dip in the wavefunction or its derivative (indicated by the dashed circle in figure 8) is a result of the different potential wells, which have their separate influences on the shape of the wavefunction, and therefore hamper the matching. The difference in $\phi(x)$ being zero (or not) can be interpreted as a generalization of matching the individual states in an asymmetric (symmetric) way when the Landau states are degenerate at $k \to \infty$.

6. Time-dependent classical interpretation

One can make various attempts to link a classical picture to quantum mechanics. Often the comparison starts with a schematic classical picture which is then supported by comparing the quantum mechanical probability density with the classical one, obtained through calculation

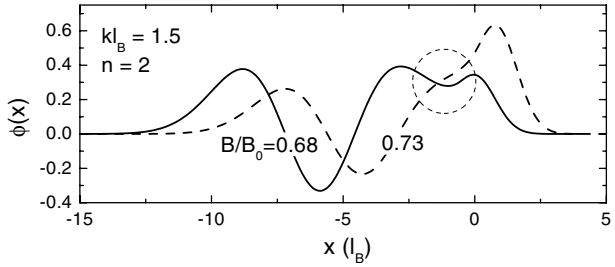

Figure 8. The wavefunctions for $kl_B = 1.5$, $n = 2$ for two negative-velocity states (see figure 6) with background magnetic field $B/B_0 = 0.68, 0.73$.

of the classical electron trajectory solving Newton's equation. For a 1D problem one can also verify the classical motion by inspection of the velocity parallel to the edge [1, 13, 16, 19]. For a cylindrically symmetric problem, the classical electron motion can be inferred from the magnetic moment or the circular current distribution of the electron state [9–12]. In this paper, a quantitative comparison was made by use of a quantum mechanical velocity parallel to the 1D magnetic field discontinuity. In the following, we will try a different approach where we will construct time-dependent states, and in doing so we will introduce another feature, i.e. the oscillation frequency perpendicular to the magnetic edge.

6.1. $B = 0$

We have already mentioned that the solutions for this kind of problem are the parabolic cylinder functions $\phi(x) = D_{E-1/2}[\sqrt{2}(x - k)]$, matched in such a way that we have symmetric and antisymmetric wavefunctions as is shown for $k = 2$ in figure 1(a). At $k = \infty$, these symmetric and antisymmetric states are twofold degenerate (see the two wavefunctions corresponding to the solid square in figure 1(a)). Due to this degeneracy any linear combination of these states is also an eigenstate. If we take the following linear combination:

$$\begin{aligned} |m_+\rangle &= \frac{1}{\sqrt{2}}(|2m\rangle + |2m+1\rangle) \\ |m_-\rangle &= \frac{1}{\sqrt{2}}(|2m\rangle - |2m+1\rangle) \end{aligned} \tag{17}$$

we arrive at the well known Landau states, i.e. wavefunctions of electrons located in two different homogeneous magnetic field profiles. One electron is moving clockwise, while the other is moving anticlockwise. For decreasing k this degeneracy is lifted. Although taking linear combinations of states with a different energies yields a time-dependent solution, we will extrapolate this picture towards all of the other states. We choose a new orthonormal but time-dependent basis:

$$\begin{aligned} |m_+\rangle &= (\mathrm{e}^{\mathrm{i}E_{2m}t}|2m\rangle + \mathrm{e}^{\mathrm{i}E_{2m+1}t}|2m+1\rangle)/\sqrt{2} \\ |m_-\rangle &= (\mathrm{e}^{\mathrm{i}E_{2m}t}|2m\rangle - \mathrm{e}^{\mathrm{i}E_{2m+1}t}|2m+1\rangle)/\sqrt{2} \end{aligned} \tag{18}$$

with $E_{m_+} = E_{m_-} = (E_{2m} + E_{2m+1})/2$. The resulting energy spectrum is shown in figure 2(a) by the dashed curves. The corresponding velocities are plotted in figure 9(a). For every branch there are two states, $|m_+\rangle$ and $|m_-\rangle$.

With these new quantum states, much better agreement is obtained with the corresponding classical results (dotted curves in figure 9(a)). Because of the addition of the two eigenstates the negative velocity has almost disappeared. Only the lowering of the energy, as was mentioned

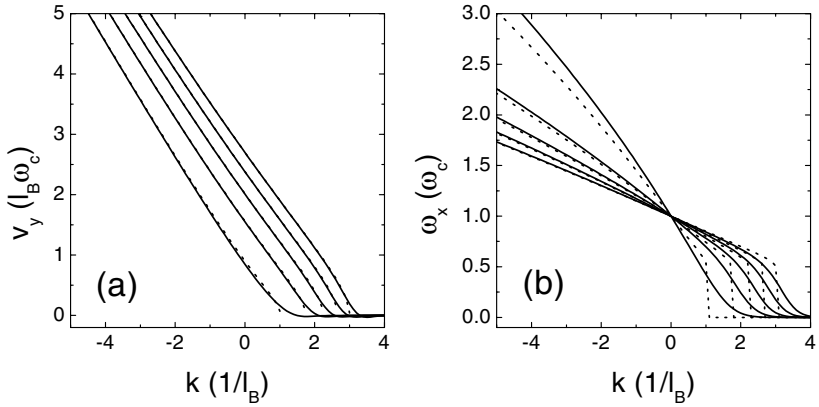

Figure 9. (a) The quantum mechanical velocity in the y-direction (solid curves) of the time-dependent states for the case $B^l = -B^r = -1$ and the velocity obtained classically (dotted curves). (b) As (a), but for the oscillation frequency in the x-direction.

for the limiting case (i.e. $k \to \infty$), results in a small negative velocity, which cannot be understood even in this picture. Also the boundary which indicates when classical states propagate is in much better agreement now.

Since we now have time-dependent states, we can calculate a new feature: the oscillation frequency ω_x in the x-direction. The time-dependent probability densities of the $|m_+\rangle$ and $|m_-\rangle$ states have the following form:

$$|\langle m_+|x\rangle(t)|^2 = \frac{1}{2}(|\langle 2m|x\rangle|^2 + |\langle 2m+1|x\rangle|^2 + 2\cos[\omega_x t]\langle 2m|x\rangle\langle 2m+1|x\rangle)$$
$$= |\langle m_-|x\rangle(t + \pi/\omega_x)|^2 \tag{19}$$

where $\omega_{x,m} = (E_{2m+1} - E_{2m})/\hbar$ is the quantum mechanical oscillator frequency in the x-direction.

Classically we can calculate this frequency ω_x, again using simple geometrical considerations, which leads to

$$\omega_x(k) = \frac{\pi}{2\arccos(-k/v_\varphi(k))}. \tag{20}$$

Both results are plotted in figure 9(b), and we obtain reasonably good agreement between the quantum (solid curves) and classical (dotted curves) results. Notice that for $|k| > k^*$, classically $\omega_x = 0$, which means that the electron does not oscillate between the two different magnetic field regions (i.e. it is not a snake orbit state), but it oscillates in a homogeneous magnetic field and consequently we obtain the time-independent eigenstates corresponding to the Landau levels.

Of course this approach is only useful if proper linear combinations are possible. Unfortunately this is not the case when a background magnetic field $B \leqslant B_0$ is applied.

6.2. $B > B_0$

The above approach is also fruitful in the case where $0 < B^l < B^r$. We can again add adjacent levels, two by two, as described before. We can repeat the earlier procedure exactly, and we arrive again at the time-dependent states of equation (18). The energy spectrum of these states when $B = 3B_0/2$ is shown in figure 2(d), by dashed curves. From figure 10(a), we notice that

the classical velocity is in better agreement than before, since the amplitude of the wiggles is lowered, due to the summation. The quantum mechanical oscillation frequency in the x-direction is again given by $\omega_{x,m} = (E_{2m+1} - E_{2m})/\hbar$ and plotted in figure 10(b). We notice that since there are no degenerate states, we always have oscillating electrons. For $k \to \infty$ the electron oscillates with frequency $\omega_x = 2.5\omega_c$, while for $k \to -\infty$ the electron oscillates with frequency $\omega_x = 0.5\omega_c$; i.e. the electrons circle around in their separate homogeneous magnetic fields. This can also be seen from the classical oscillation frequency in the x-direction, which is given by

$$\omega_x(k) = \pi \left[\frac{\arccos(k/v_\varphi(k))}{B^l} + \frac{\arccos(-k/v_\varphi(k))}{B^r} \right]^{-1}. \tag{21}$$

Notice that also here wiggles in v_y are present (see figure 10(b)) which are not present in the classical results. It is clear that proper linear combinations can always be constructed, as long as $B > B_0$.

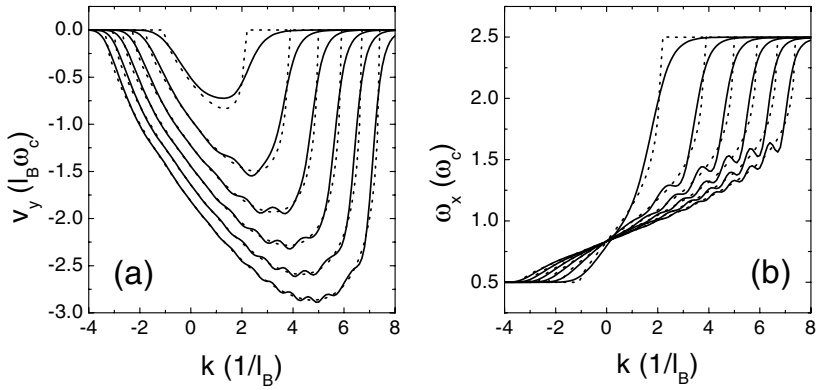

Figure 10. As figure 9, but for the magnetic field profile with $(B^l, B^r) = (0.5, 2.5)$.

7. Conclusions

We studied the electron states near discontinuities in the magnetic field. Different 1D magnetic field profiles, i.e. steps, were considered. The quantum mechanical energy spectrum was obtained and the group velocity of the states was calculated. Their corresponding classical orbits were found and the propagating states which are located at the magnetic field discontinuity correspond to snake orbits. Quantum mechanical magnetic edge states were found which move along the magnetic field step in the opposite direction to the classical snake orbits and which cannot be understood classically. We were able to construct non-stationary quantum mechanical states which closely approximate the classical solution for the symmetrical case $B^l = -B^r$ and for the more general case $B^r > B^l > B_0$.

The characteristics of the electron states, e.g. their energy, velocity and position, play an important role in the electron transport and in fact they are used as input in conductivity calculations. Recently Nogaret *et al* [22] realized an experiment in which a ferromagnetic stripe was placed on top of a quantum wire parallel to the wire axis. If magnetized perpendicularly, the fringe fields of the stripe induce an alternating magnetic field in the wire, and snake orbits propagate underneath its edges. As a function of the applied background field, a resonance peak in the magnetoresistance and the differential Hall resistance was measured, which was

explained as due to the destruction of the snake orbits with increasing background magnetic field. We recently reviewed [23] this theoretical explanation and found that this picture has to be supplemented with the normal edge states in order to find the correct magnetic field position of the resonance peak.

In future experimental set-ups it might be possible to inject a chosen k-vector for a particular energy, by use of a sort of k-dependent filter, like Matulis *et al* [17] suggested. This would allow one to selectively populate the different orbital states.

Acknowledgments

This work was partially supported by the Inter-university Micro-Electronics Centre (IMEC, Leuven), the Flemish Science Foundation (FWO-Vl), BOF-GOA and the IUAP-IV. JR was supported by 'het Vlaams Instituut voor de bevordering van het Wetenschappelijk & Technologisch Onderzoek in de Industrie' (IWT) and FMP is a research director with the FWO-Vl. We acknowledge fruitful discussions with A Matulis, P Vasilopoulos, S Badalian and J A Tyszynski.

References

[1] Peeters F M and De Boeck J 1999 *Handbook of Nanostructured Materials and Technology* vol 3, ed N S Nalwa (New York: Academic) p 345
[2] Foden C L, Leadbeater M L, Burroughes J H and Pepper M 1994 *J. Phys.: Condens. Matter* **6**
[3] Smith A, Taboryski R, Hansen L T, Sørensen C B, Hedegård P and Lindelof P E 1994 *Phys. Rev.* B **50** 14 726
[4] Geim A K, Grigorieva I V, Dubonos S V, Lok J G S, Maan J C, Filippov A E and Peeters F M 1997 *Nature* **390** 259
[5] Dubonos S V, Geim A K, Novoselov K S, Lok J G S, Maan J C and Henini M 2000 *Physica* E **6** 746
[6] Kubrak V, Rahman F, Gallagher B L, Main P C, Henini M, Marrows C H and Howson M A 1999 *Appl. Phys. Lett.* **74** 2507
[7] Johnson M, Bennett B R, Yang M J, Miller M M and Shanabrook B V 1997 *Appl. Phys. Lett.* **71** 974
Monzon F G, Johnson M and Roukes M L 1997 *Appl. Phys. Lett.* **71** 3087
Reijniers J and Peeters F M 1998 *Appl. Phys. Lett.* **73** 357
[8] Reijniers J, Matulis A and Peeters F M 2000 *Physica* E **6** 759
[9] Solimany L and Kramer B 1995 *Solid State Commun.* **96** 471
[10] Sim H-S, Ahn K-H, Chang K J, Ihm G, Kim N and Lee S J 1998 *Phys. Rev. Lett.* **80** 1501
[11] Reijniers J, Peeters F M and Matulis A 1999 *Phys. Rev.* B **59** 2817
[12] Kim N, Ihm G, Sim H-S and Chang K J 1999 *Phys. Rev.* B **60** 8767
[13] Müller J E 1992 *Phys. Rev. Lett.* **68** 358
[14] Peeters F M and Vasilopoulos P 1993 *Phys. Rev.* B **47** 1466
[15] Ibrahim I S and Peeters F M 1995 *Am. J. Phys.* **63** 171
[16] Zwerschke S D M, Manolescu A and Gerhardts R R 1999 *Phys. Rev.* B **60** 5536
[17] Peeters F M and Matulis A 1993 *Phys. Rev.* B **48** 15 166
Matulis A, Peeters F M and Vasilopoulos P 1994 *Phys. Rev. Lett.* **72** 1518
[18] Calvo M 1993 *Phys. Rev.* B **48** 2365
[19] Gu B-Y, Sheng W-D, Wang X-H and Wang J 1997 *Phys. Rev.* B **56** 13 434
[20] Peeters F M, Reijniers J, Badalian S M and Vasilopoulos P 1999 *Microelectron. Eng.* **74** 405
[21] Man'kov Y I 1972 *Sov. Phys.–Solid State* **14** 62
Balkarei Y I and Bulaevskii L N 1973 *Sov. Phys.–Solid State* **14** 2018
Rozhavsky A S and Shekhter R I 1973 *Solid State Commun.* **12** 603
Cabrera G G and Falicov L M 1974 *Phys. Status Solidi* b **61** 539
Cabrera G G and Falicov L M 1974 *Phys. Status Solidi* b **62** 217
Berger L 1978 *J. Appl. Phys.* **49** 2156
Zakharov Y V and Man'kov Y I 1984 *Phys. Status Solidi* b **125** 197
[22] Nogaret A, Bending S J and Henini M 2000 *Phys. Rev. Lett.* **84** 2231
[23] Reijniers J and Peeters F M 2000 unpublished